Integration of oxalic acid chelation and Fenton process for synergistic relaxation-oxidation of persistent gel-like fouling of ceramic nanofiltration membranes

Lin, Bin; Heijman, Sebastiaan G.J.; Shang, Ran; Rietveld, Luuk C.

DOI
10.1016/j.memsci.2021.119553

Publication date
2021

Document Version
Final published version

Published in
Journal of Membrane Science

Journal of Membrane Science 636 (2021) 119553

Contents lists available at ScienceDirect

Journal of Membrane Science

journal homepage: www.elsevier.com/locate/memsci

Integration of oxalic acid chelation and Fenton process for synergistic relaxation-oxidation of persistent gel-like fouling of ceramic nanofiltration membranes

Bin Lin [a,*], Sebastiaan G.J. Heijman [a], Ran Shang [b], Luuk C. Rietveld [a]

[a] Department of Water Management, Faculty of Civil Engineering and Geosciences, Delft University of Technology, Stevinweg 1, 2628 CN Delft, The Netherlands
[b] Veolia Water Technologies Techno Center Netherlands B.V., Tanthofdreef 21, 2623 EW Delft, The Netherlands

ARTICLE INFO

Keywords:
Ceramic membrane
Nanofiltration
Membrane fouling
Cleaning
Fenton oxidation

ABSTRACT

Ceramic nanofiltration (NF) is a newly-developed technology for water recycling, but is still limited to pilot-scale applications. Lacking efficient and eco-friendly strategies for cleaning ceramic NF membrane impedes its scaling-up in industries. Forward flush, backwash and acidic/caustic cleaning are not efficient enough. In this work, a novel oxalic acid-aided Fenton process was proposed for synergistic relaxation/oxidation of persistent Ca^{2+}-mediated gel-like fouling of ceramic NF membrane. A reactive catalyst layer was online pre-coated on top of the membrane via a pressure-driven cross-flow pre-filtration of Fe_3O_4 hydrosols. The gel-like fouling was simulated by alginate in the presence of Ca^{2+} ions. Results show that the Fe_3O_4 loading could be readily tuned from 0.16 to 1.34 g m^{-2} by altering the permeate flux during the pre-coating. The membrane permeability loss due to the pre-coating was minimal (<10%). The combination of oxalic acid chelation and Fenton-based oxidation resulted in high flux recovery (85.07%) for the iron-oxide pre-coated membrane, whereas the single treatment by hydrogen peroxide (H_2O_2) or oxalic acid was inefficient. This synergistic effect was attributed to relaxation of the Ca^{2+}-mediated gel layer via oxalic acid/Ca^{2+} chelation, which presumably facilitated H_2O_2 diffusion at the Fe_3O_4/foulant interface. The iron-oxide pre-coated membrane maintained stable initial normalized fluxes (83.33–90.15%) through the oxalic acid/H_2O_2 cleaning over five cycles, with no need of refreshing the iron-oxide pre-coat. Additionally, the leaching of iron from the iron-oxide pre-coat by oxalic acid was suppressed by the oxalic acid/H_2O_2 combination, owing to a reactive shielding by competitive sorption of H_2O_2 onto the Fe_3O_4 surface. Overall, the synergistic relaxation/oxidation method, demonstrated in this study, provides new insights into improving reactivity of Fenton-based processes on hybrid catalytic ceramic membranes for water treatment or fouling control.

1. Introduction

Ceramic nanofiltration (NF) has emerged as an attractive new technology for non-potable water recycling from municipal sewage and secondary wastewater effluent, given its good robustness and separation capability upon various organic molecules (>450 Da) and small colloids [1,2]. Formation of a low permeable gel layer on the surface of ceramic NF membranes during filtration, plays a significant role in the membrane fouling, which affects the water-yielding capacity and energy consumption in water treatment [3,4]. Typically, polysaccharides (i.e., alginate) are considered to be a major contributor to the gel layer formation, attributing to the strong bridging between carboxylic groups of the polysaccharide molecules and divalent or multivalent metal ions (i.e., Ca^{2+} and Fe^{3+}) [5–7]. Regardless of the hydrophilic surface (contact angle: 20–30°) of ceramic NF membranes, forward flush is ineffective for the gel-type fouling due to its strong adherence to the membrane [4,8]. Backwash cannot be applied to ceramic NF membranes because of physical damage to the end-sealing under high transmembrane pressures (TMP), in addition, the backwash velocity is limited at pressures below 10 bar [9]. Therefore, off-line chemical cleaning of the membranes with alkaline, acid, or hypochlorite is frequently needed, disrupting the continuous filtration and influencing the membrane integrity [10,11]. In addition, chemical cleaning agents, such as NaOH and citric acid, are incapable of fully eliminating the foulants even if the

* Corresponding author.
E-mail address: b.lin@tudelft.nl (B. Lin).

https://doi.org/10.1016/j.memsci.2021.119553
Received 8 March 2021; Received in revised form 31 May 2021; Accepted 24 June 2021
Available online 29 June 2021

flux was entirely recovered, leading to a progressive flux decrease with successive filtration cycles [4].

Membrane modification with Fenton catalysts enables foulant removal on the membrane surface via on-site generation of reactive oxygen species (i.e., $^{\bullet}OH$), after addition of hydrogen peroxide (H_2O_2) [12]. The co-existence of catalysts, H_2O_2 and foulants on a catalyst-modified membrane surface could create conditions that are favourable for fouling layer decay, because of the short diffusive transport distance in Fenton oxidation processes at the catalyst/foulant interface [13]. The Fenton oxidation processes on the membrane surface aim to attack the anchoring sites at the catalytic membrane/foulant interface, which would result in fouling layer detachment. De Angelis and de Cortalezzi reported that Fenton reactions on an iron-oxide modified ceramic membrane achieved a flux recovery of 80% with bovine serum albumin degradation percentage of 40%, indicating an underlying detachment or relaxation of the fouling layer by Fenton oxidation [14]. According to Sun et al. UV/H_2O_2 photo-Fenton oxidation on a α-FeOOH-coated ceramic membrane was able to limit the increase of TMP to a plateau level, during continuous filtration of humic acid solutions [15]. Above mentioned studies, however, only have paid attention to the viability of using membrane-surface-localized Fenton reactions for fouling control, but in water treatment by ceramic membranes, a persistent fouling layer (i.e., gel-like foulants) on the membrane surface may affect the reactivity of Fenton processes, which is still unresolved and poorly understood [14,15].

Accumulation of foulants on catalytic membranes shortens the mass transfer distance of $^{\bullet}OH$ for foulant decay, which, in principle, is favourable for catalysed oxidation on the membrane surface [16]. However, the fouling layer itself, as an undesirable steric barrier, could limit the diffusive transport of H_2O_2 onto the catalytic sites and hamper the oxidation of foulants. In particular, the gel layer composed of biopolymers (i.e., polysaccharides) on the membrane surface could act as a mass transfer hindrance [17]. With the aid of Ca^{2+} ions, ubiquitous in natural water bodies, the cross-linked networks of the gel layer would be further intensified and compressed under pressure-driven filtration, due to intermolecular bridging between foulant molecules or charge screening by Ca^{2+} [5,18]. As such, the Ca^{2+}-mediated gel-like fouling layer, with low permeability, affects the application of Fenton-coupled ceramic membranes for water treatment or fouling control in practice [3,19]. Therefore, H_2O_2 mass transfer on catalyst-immobilized membranes should be improved to enhance Fenton oxidation for fouling control.

Ligand exchange reactions, governed by chelating agents, are capable of extracting Ca^{2+} from the Ca^{2+}-mediated gel layer, rendering a relaxed conformation of the gel layer through resuming intra- or intermolecular or foulant-membrane electrostatic repulsion or destructing intermolecular bridging [20]. As such, loosening fouling layer structures could also be expected as a factor contributing to flux recovery, in addition to removing the fouling layer from membrane surfaces. Nonetheless, Song et al. has reported that chelating agent cleaning might be ineffective for Ca^{2+}-unbound foulant molecules, which are generally protonated under acidic conditions [21]. As reported by Athanasekou et al., ceramic NF membranes, with alginate deposited on their surfaces, would undergo an evident permeability drop (~50%) upon exposure to divalent metal cations, due to pore narrowing/blocking induced by complexation between the divalent metal cations and alginate's carboxylic groups [22]. It can thus be speculated that some residual foulants on membranes, after Ca^{2+} extraction through chelation cleaning, could release their binding sites (i.e., carboxylic groups) for free metal cations (i.e., Ca^{2+}) in aqueous phase, which might reorganize cross-linked gel networks on the membranes and lead to a flux decline upon exposure to Ca^{2+}. Additionally, some foulants, tightly embedded in the concavities or pore-openings of membrane surfaces, were not amendable to chelation cleaning [21,23].

In this study, a novel synergistic method of using chelating-agent relaxation and Fenton-based oxidation was proposed, for cleaning persistent gel-like fouling of ceramic NF membranes. Fe_3O_4 hydrosol nanoparticles were adopted as active Fenton catalysts to form an iron-oxide pre-coat on the membrane surface prior to fouling, due to their capability of triggering Fenton-based oxidation and facile synthesis processes. Sodium alginate, which is known to form gel aggregates through a so-called egg-box model in the presence of calcium ions, was chosen as a representative gel-like foulant to develop a gel layer on the membranes [5,11]. As suggested by pre-coated membranes prepared by particle materials (i.e., iron oxide and powdered activated carbon) reported elsewhere, the gel foulants are supposed to be deposited on top of the iron-oxide multilayer and within its porous channels [24,25]. Oxalic acid was used to assist the Fenton-oxidative cleaning of the iron-oxide pre-coated membranes, in light of its functions of complexing with Ca^{2+}-mediated gel layer and good resistance to $^{\bullet}OH$-radical oxidation [26].

2. Materials and methods

2.1. Chemicals and membranes

Ferric chloride hexahydrate ($FeCl_3{\cdot}6H_2O$, ≥99.0%), ferrous chloride ($FeCl_2$, ≥98.0%), sodium alginate (≥99.0%) and oxalic acid ($C_2H_2O_4$, ≥99.0%) were purchased from Sigma-Aldrich. H_2O_2 (30%), calcium chloride dihydrate ($CaCl_2{\cdot}2H_2O$, ≥99.0%), H_2O_2 test kits (limit of detection (LOD): 0.03–6 mg L^{-1}) and iron test kits (LOD: 0.10–5 mg L^{-1}) were purchased from Merck (Germany). All chemicals were used as received. Commercially available TiO_2 NF membranes (Inopor GmbH, Germany) with nominal molecular weight cut-off of 450 Da and mean pore size of 0.9 nm were used in this study (Table S1). The membranes have a single channel and a tubular configuration with dimensions of 10 mm in outer diameter, 7 mm in channel diameter and 100 mm in length. The effective filtration area of each membrane is 0.00163 m^2. The membranes were sealed with epoxy glue on the membranes edges to avoid feed water passing through the edges prior to use. The membranes were operated in an inside-out mode during filtration.

2.2. Synthesis of iron oxide hydrosol nanoparticles

Wet-state Fe_3O_4 hydrosol catalysts were synthesized with the sol-gel method [27]. In brief, 4.00 g $FeCl_2$ and 17.07 g $FeCl_3{\cdot}5H_2O$ were successively dissolved into 0.1 L of a 0.60 M HCl solution. The acidified solution of ferrous/ferric ions (Fe(II)/Fe(III)) was then dropwise added into 2.0 L of a 0.15 M NaOH solution with continuously stirring at a speed of 200 rpm, until the solution reached a pH of 2.5. The obtained black Fe_3O_4 hydrosols appeared well suspended and dispersed, which were favourable for iron-oxide pre-coating through pressure-driven pre-filtration processes. The Fe_3O_4 hydrosols were stored in a fridge at 4 °C prior to use.

2.3. Integrative pre-coating/filtration/cleaning system

Catalyst pre-coating, fouling and cleaning of ceramic NF membranes were operated in an integrative apparatus (Fig. 1). Fe_3O_4 hydrosols were used for the catalyst pre-coating through a cross-flow filtration to in situ form a uniform iron-oxide pre-coat on the membrane surface. The Fe_3O_4 suspension (47.0 mM) was spiked into a demineralized water feed stream and the pre-coating filtration was operated at TMP of 2.0–10.0 bar and at a cross-flow velocity of 0.65 m s^{-1} for 30 min. Laminar cross-flow inside the membrane channel was adopted to promote Fe_3O_4 deposition onto the membrane surface. The Fe_3O_4 loading on the membranes, ahead of fouling/cleaning experiments, was determined by fully dissolving the iron oxide pre-coat with oxalic acid solutions and measuring the dissolved iron. For a ceramic NF membrane with a specific permeability, the Fe_3O_4 loading can be readily reproduced by tuning permeate volume during Fe_3O_4 pre-filtration under a certain TMP. Therefore, the Fe_3O_4 loading amount, measured before batch

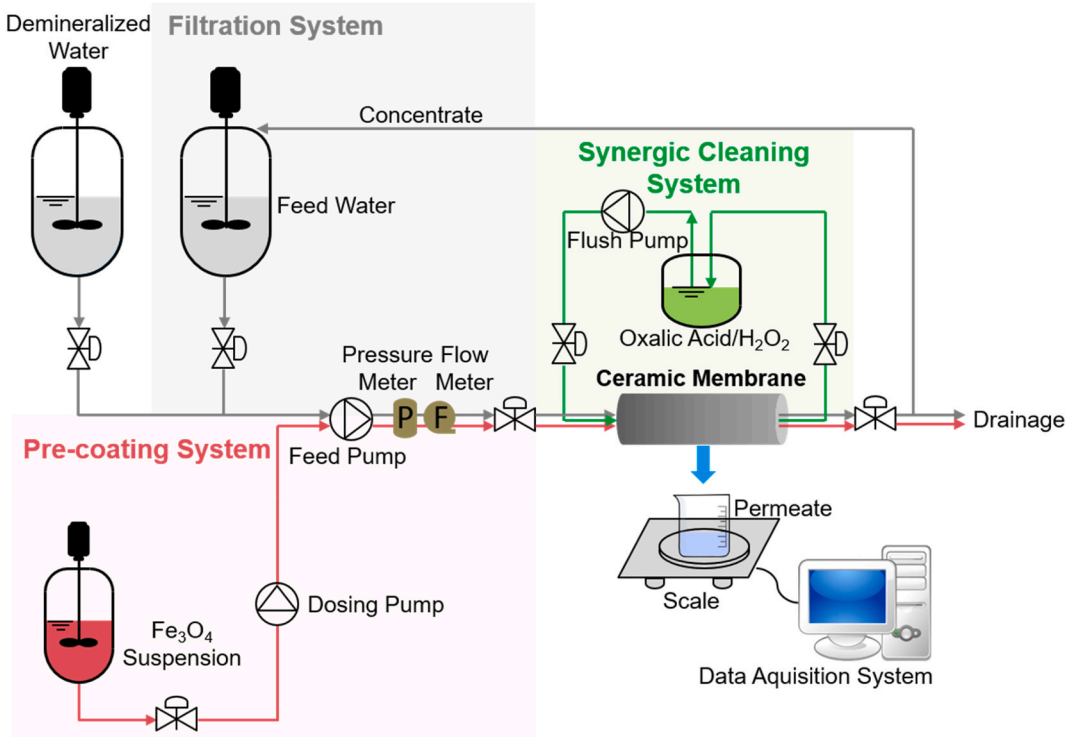

Fig. 1. Schematic of integrative pre-coating/filtration/cleaning system of ceramic nanofiltration membrane.

experiments, can be regarded as the initial iron loading. The deposition and packing of Fe_3O_4 nanoparticles largely relied on the permeate flux and cross flow velocity [28], which determined the mass transported to the membrane surface (nominal Fe_3O_4 loading) and the mass swept away from the membrane (Fe_3O_4 loss), respectively. The nominal loading mass and coating efficiency of Fe_3O_4 nanoparticles could be calculated as described in Text S1.

Fouling processes were conducted after the iron oxide pre-coating of ceramic NF membranes, using a synthetic foulant sodium alginate. NaCl (5.0 mM) and $CaCl_2$ (3.0 mM) were added into sodium alginate solutions (0.8 g L^{-1}) to simulate the solution chemistry of natural waters. $NaHCO_3$ (1.0 mM) was added to maintain pH 7.0 (Text S2). Filtration was carried out in a bench-scale cross-flow mode (Fig. 1). Prior to fouling tests, the pristine and iron-coated membranes were pre-compacted with demineralized water under 3.0 bar until a stable flux was reached. The membranes were then stabilized with demineralized water for 10 min to determine the stable initial permeate flux (J_0). During the fouling experiments, the retentate was recycled to the feed tank (50 L), while the permeate was collected continuously for measuring the permeate flux. The filtration experiments were executed at a constant TMP of 3.0 bar with initial fluxes of >50 L m^{-2} h^{-1} during fouling, which should be a regular flux for ceramic NF and sufficient for the formation of gel fouling with concentrated alginate solutions [29]. A cross-flow velocity of 1.0 m s^{-1} was adopted during the fouling experiments (for 60 min). The Reynolds number of 6116 was used during the filtration to create turbulent conditions. In the filtration tests with the iron-oxide pre-coated membranes, the content of total iron in the permeate side was lower than the detection limit of 0.1 mg L^{-1}, which is below the permissible limit of iron in drinking water (0.3 mg L^{-1}, WHO standard) [30].

Membrane cleaning was performed by circulating a mixed solution of oxalic acid/H_2O_2 in the feed channel as illustrated in Fig. 1. The cleaning performance was evaluated by tracking the permeate flux over multiple filtration cycles. An oxalic acid/H_2O_2 solution with 30.0 mM H_2O_2, 11.1 mM oxalic acid and pH 2.5 were adopted, corresponding to the optimum value for Fenton cleaning based on previously executed optimization tests (data not shown). Herein, as suggested by Mailen et al., degradation of oxalic acid by H_2O_2 could be assumed negligible due to the slow reaction rate ($k < 2.8 \times 10^{-6}$ M^{-1} s^{-1}) at 20 °C [31]. Membrane cleaning in our experiments was conducted at a low cross-flow velocity (0.02 m s^{-1}), in order to reduce the hydraulic scouring on the iron-oxide pre-coat. Each fouling/cleaning cycle consisted of four sequential steps: a) permeate flux test using demineralized water, b) filtration of the synthetic foulant solution, c) membrane cleaning with the oxalic acid and/or H_2O_2 solution, and d) permeate flux test using demineralized water. Cleaning with only oxalic acid or H_2O_2, or with a combination of oxalic acid and H_2O_2 were conducted in parallel for the pristine and Fe_3O_4-coated membranes, respectively, in order to separately explore the individual roles of oxalic acid and H_2O_2 in the synergistic oxalic acid-assisted Fenton cleaning. Afterwards, the cleaned membranes were soaked into a $CaCl_2$ solution (3.0 mM, pH 7.0), then the flux decline upon Ca^{2+} exposure (for 12 h) was investigated to evaluate the foulant removal from the membrane surface, since re-compaction of remaining foulants could occur and form again a compact layer due to Ca^{2+} complexation. Flux recovery ratios after membrane cleaning were calculated using Eq. (1).

$$F_r = \frac{J_c - J_f}{J_w - J_f} \times 100\% \tag{1}$$

where J_c (L m^{-2} h^{-1}) is the flux of demineralized water after cleaning, J_w (L m^{-2} h^{-1}) represents the initial flux of demineralized water prior to fouling tests, and J_f (L m^{-2} h^{-1}) is designated to the water flux after membrane fouling. The filtration/cleaning experiments were performed in duplicate, and the variations in terms of membrane permeance before/during fouling or after cleaning were within a 5% difference.

Multicycle fouling/cleaning experiments were also conducted at bench scale, with a fouling duration of 60 min and cleaning time of 15 min in each cycle. The unified membrane fouling index (*UMFI*) was used to quantitatively assess the total fouling and chemically irreversible fouling of the iron-oxide pre-coat with the oxalic acid-coupled Fenton cleaning. A detailed description of the *UMFI* has been provided elsewhere [32]. The *UMFI* was defined as a slope in the linear equation given

in Eq. (2).

$$\frac{1}{J_s'} = 1 + (UMFI) \times V_s \quad (2)$$

where *Js'* is the normalized specific permeate flux, and *Vs* (L m^{-2}) represents the unit permeate volume. A higher *UMFI* (m^2 L^{-1}) value implies a faster decrease of *Js'*. Herein, the total fouling refers to the membrane fouling before hydraulic or chemical cleaning, and the chemically irreversible fouling denotes the residual fouling after chemical cleaning (oxalic acid/H_2O_2 cleaning). The total fouling index (*TFI*) was further calculated by a linear regression of fouling data of each filtration cycle. The chemically irreversible fouling index (*CIFI*) was finally determined by collecting the starting points of each filtration cycle by linear regression. The two-point approach, using the starting points of the first and final cycles, was also adopted for comparison [32].

Real surface water was also fed to the iron-oxide pre-coated ceramic NF membrane to test the applicability of the oxalic acid-aided Fenton-based cleaning strategy in practice. Canal water was collected at the Delftse Schie (Delft, the Netherlands) and pre-filtrated with a fine sieve of 1 mm mesh width before NF. Key water quality parameters of the canal water are summarised in Table S2. It should be noted that the fouling with alginate solutions is an accelerated fouling with a much higher load (0.8 g L^{-1}) than that of the pilot experiment in canal water treatment (11.9 mg L^{-1}, Table S2). As suggested by one of our previous studies, using this model solutions, a pilot fouling experiment of five days could be simulated in 2 h, due to the faster fouling by the concentrated alginate solutions [2].

2.4. Characterization of iron oxide nanoparticles and membranes and analysis of water quality

Morphologies of Fe_3O_4 nanoparticles and top/cross-sectional views of iron-coated membranes were observed by transmission electron microscope (TEM, JEM-2100 HR, JEOL, Japan) and scanning electron microscopy (SEM, Hitachi S-3400 II, Japan) equipped with energy dispersive spectroscopy (EDS). X-ray diffraction (XRD) was performed with an XRD diffractometer (D8-Advance, Bruker, USA) with Cu Kα radiation at 45 kV and 40 mA. Specific surface area was determined by N_2 adsorption-desorption tests at 77 K (ASAP-2010C, Micromeritics Instrument, USA). The standard Brunauer-Emmett-Teller model was used to calculate the surface area (S_{BET}) of the dried particles. Average particle size of Fe_3O_4 nanoparticles was estimated based on the S_{BET} value presuming a spherical morphology of the Fe_3O_4 (Text S3). Dissolved organic carbon (DOC) was determined by a total organic carbon analyser (TOC-VCPH, Shimadzu, Japan). The ions in the canal water samples were measured by ion chromatography (883 Basic IC plus, Metrohm Instrument, the Netherlands). UV_{254} was determined by UV/vis spectrometer (GENESYS 10S UV–Vis, Thermo Scientific, USA) with a quartz cell (1 cm). Fe Leaching of iron oxide pre-coat was measured in a photometer (Spectroquant NOVA 60, Merck KGaA, Germany) using iron test kits. H_2O_2 concentration was measured by hydrogen peroxide test kits. During each test, the samples were filtered through 0.45 μm filters to retain possible impurities.

2.5. Iron leaching of iron-oxide pre-coated membranes

Stability and Fenton-based (homogeneous or heterogeneous) reactions are greatly dependent on the Fe leaching of iron-oxide pre-coat. To understand the iron leaching, the dissolution of iron from the iron-oxide pre-coat was explored during the membrane cleaning with sole oxalic acid (or H_2O_2) and oxalic acid/H_2O_2 combination. The iron-oxide pre-coated membranes were subjected to Ca^{2+}-alginate fouling with varying durations (i.e., 1 and 3 h) to simulate actual conditions of iron leaching during membrane cleaning. The iron leaching tests were performed at 20 °C and pH 2.5. Aliquots of 8.0 mL were withdrawn at selected time intervals and filtered for analysing the Fe concentration to determine the iron dissolution rate of the iron-oxide pre-coat. During batch cleaning, the dissolved (or fallen) iron was detected, which could be used for determining the loss amount of Fe_3O_4 from the membrane in cleaning processes. For determining the iron loss during the H_2O_2 batch cleaning, oxalic acid was introduced into H_2O_2 solutions after the batch cleaning so as to entirely dissolve the fallen Fe_3O_4 solids, which assured that all the lost iron could be measured as Fe(II) or Fe(III) ions. In order to study the possible competition between H_2O_2 and oxalic acid towards the active sites on the Fe_3O_4 catalytic layer, adsorption of oxalic acid was conducted in the absence and presence of H_2O_2. To exclude the interference of ceramic membrane, the solid particles, dried from Fe_3O_4 hydrosols, were used for the adsorption experiments. The Fe_3O_4 particles (1.0 g L^{-1}) were mixed and stirred with oxalic acid (0.55 and 11.0 mM) at pH 2.5 in the absence and presence of H_2O_2 (30.0 mM). The loading of oxalic acid on the Fe_3O_4 powders was determined based on mass balance.

3. Results and discussion

3.1. Characterization of iron-oxide pre-coated membranes

Fig. 2a shows that the Fe_3O_4 hydrosol nanoparticles were suspended and well-dispersed in aqueous solutions, supplying good characteristics for Fe_3O_4 pre-coating. Spherical configurations were observed for most Fe_3O_4 nanoparticles with diameters <20 nm, a minor fraction of the nanoparticles exhibited a distinctive acicular-like structure that might be typical for goethite nanorods (Fig. 2a) [33]. The average particle size of the Fe_3O_4 nanoparticles was 12.72 nm (Table S3) larger than the nominal pore size (0.9 nm on average, provided by the manufacturer, Table S1) of the membranes, indicating that the Fe_3O_4 nanoparticles could be successfully deposited onto the membrane surface without penetrating into the membrane pores. As depicted in Fig. 2c, e and g, the membranes pre-filtered with Fe_3O_4 nanoparticles at higher TMP (6.0 and 10.0 bar) presented thicker (3.0 and 4.7 μm, respectively) and more uniform iron-oxide layers than that formed at 2.0 bar (1.1 μm in thickness, nonuniform), probably attributing to a larger permeate volume and greater compaction effect under the higher pressures. Additionally, the Fe_3O_4 layers (1.1–4.7 μm) appeared to be much thicker than that of the TiO_2 active layer (~50 nm, supplied by the manufacturer), suggesting that the abundant nanostructured and interconnected channels, stacked by the Fe_3O_4 nanoparticles on the membrane surface, could also act as a pre-filtration media before filtration over the active layer. As such, the Fe_3O_4 layer could be used as a protective film to alleviate the fouling of the membranes in water treatment [34]. According to the top-view SEM image (Fig. 2b), the pristine membrane displayed a dense smooth active layer surface with no apparent defects on the top surface. The iron-oxide pre-coated membranes, however, had relatively rough surfaces (Fig. 2d, f and h). The iron-oxide layers prepared at 6.0 and 10.0 bar exhibited more homogeneous surfaces than that formed at 2.0 bar.

3.2. Iron oxide loading and its impact on permeability of ceramic NF membranes

As shown in Fig. 3a, the actual loading of Fe_3O_4 (0.16–1.34 g m^{-2}) appeared to be somewhat smaller than estimates (0.33–1.70 g m^{-2}) through Fe_3O_4 retention during the cross-flow filtration, determined by the permeate volume and Fe_3O_4 concentration (13.02 ± 0.62 mg L^{-1}) in the feed (Text S1). This was probably because the permeate flow inclined to deposit the Fe_3O_4 nanoparticles onto the membrane surface to form a cake layer, while the shearing force of cross-flow tended to flush away the accumulated particles, to some extent lowering the actual Fe_3O_4 loading on the membranes [35]. Herein, measurement of Fe_3O_4 loss was also considered when determining the actual loading amount of Fe_3O_4 nanoparticles (Text S1), in order to optimize TMP for improving

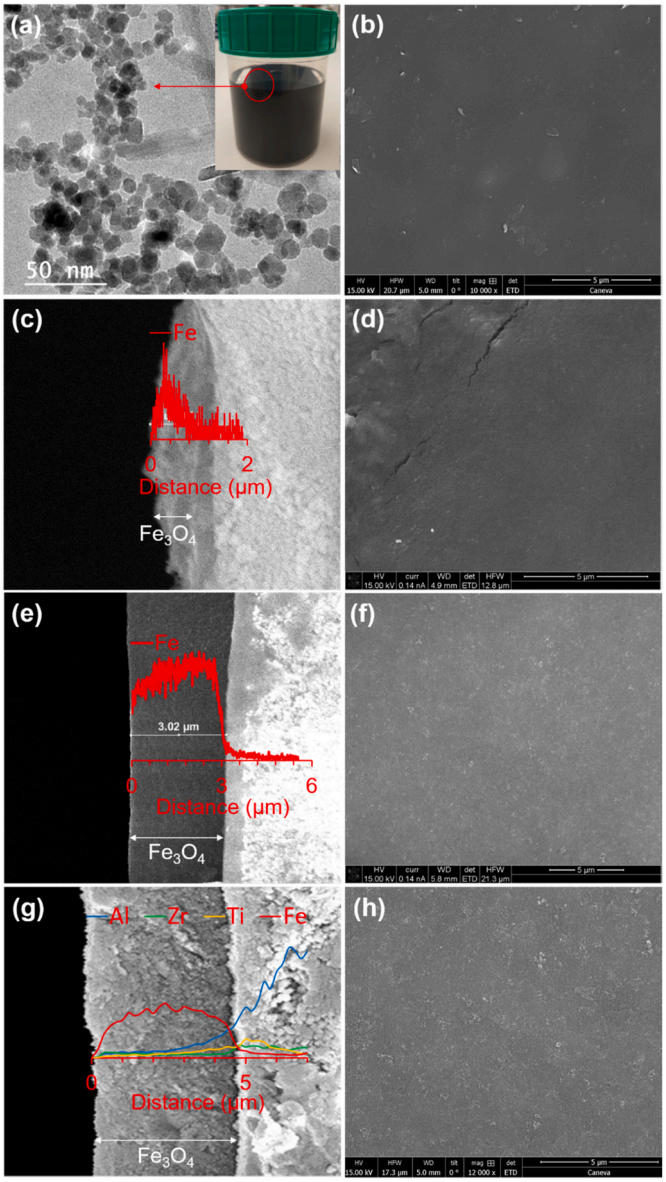

Fig. 2. Characterization of Fe_3O_4 hydrosols and ceramic nanofiltration membranes: (a) TEM image of Fe_3O_4 hydrosol nanoparticles. (b) Top-view SEM image of pristine membrane. Cross-section SEM images with inset EDS profiles and top-view SEM images of iron-oxide pre-coated membranes prepared at (c, d) 2.0 bar, (e, f) 6.0 bar and (g, h) 10.0 bar.

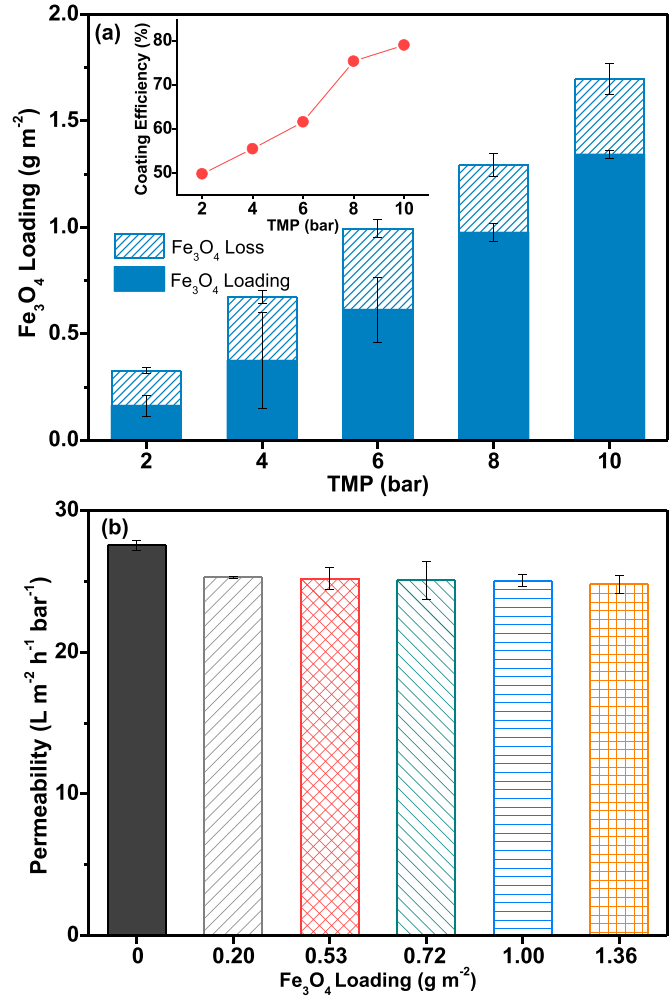

Fig. 3. (a) Fe_3O_4 loading during pre-coating filtration at different transmembrane pressures (TMP). Inset: Fe_3O_4 coating efficiency vs. applied TMP. (b) Effect of Fe_3O_4 loading on the permeability of iron-oxide pre-coated membranes. Error bars represent standard deviation of the values in duplicate.

coating efficiency. The actual loading of Fe_3O_4 was positively related to the TMP, suggesting that a higher permeate flux was more favourable for Fe_3O_4 deposition on the membrane surface. Under each filtration TMP, it was inevitable to lose a part of Fe_3O_4 particles due to the shearing force of cross-flow filtration, but the proportion of the Fe_3O_4 mass loss was decreased from 50.20% to 20.86% with increasing the TMP from 2.0 to 10.0 bar. Thus, the coating efficiency was successfully improved from 49.80% to 79.14% by a higher operating TMP, as indicated by the inset of Fig. 3a.

As depicted in Fig. 3b, in comparison with the pristine membrane, the Fe_3O_4 loading of 0.20 g m^{-2} decreased the membrane permeability by only 8.18%. Subsequently, the permeability reached a plateau even when the Fe_3O_4 loading was further increased to 1.36 g m^{-2} (adopted in our experiments), which led to a permeability decline of 9.98%. The low influence of the iron-oxide loadings (or thickness) on the demineralized water permeance of the membrane could be interpreted by the much higher porosities (>0.9, Text S4) of the iron-oxide layers than that of the supporting membrane (0.3–0.4, provided by the manufacturer). In contrast to the stable permeability of ceramic NF membranes (~25 L m^{-2} h^{-1} bar^{-1}) loaded with different amounts of Fe_3O_4 (0.20–1.36 g m^{-2}), pre-coating of microfiltration (MF) and ultrafiltration (UF) membranes, as earlier reported, produced a sharp decline in membrane permeability (by ~90%) after coating with nanoparticles (i.e., multi-walled carbon nanotubes and magnesium hydroxides), due to a rapid pore blockage of the membranes [36,37]. The Fe_3O_4 coating layer on the ceramic NF membranes was expected to be sufficiently porous with gaps between the particles larger than the membrane pore size due to the much larger size of the Fe_3O_4 particles (12.72 nm) than that of the nominal membrane pores (0.9 nm), which correspondingly provided interconnected channels for maintaining a steady water permeation. This advantage of ceramic NF membranes made it feasible to tune catalyst loading on the membranes without considerable loss of membrane permeability, in order to supply adequate active sites for catalysed reactions on the membrane surface.

3.3. Fenton oxidative cleaning of iron-oxide pre-coated membranes without using oxalic acid

As observed in Fig. 4a, the permeate flux of both the pristine and iron-oxide pre-coated membranes underwent an abrupt drop during the initial stage of fouling with Ca^{2+}-alginate solutions, probably due to

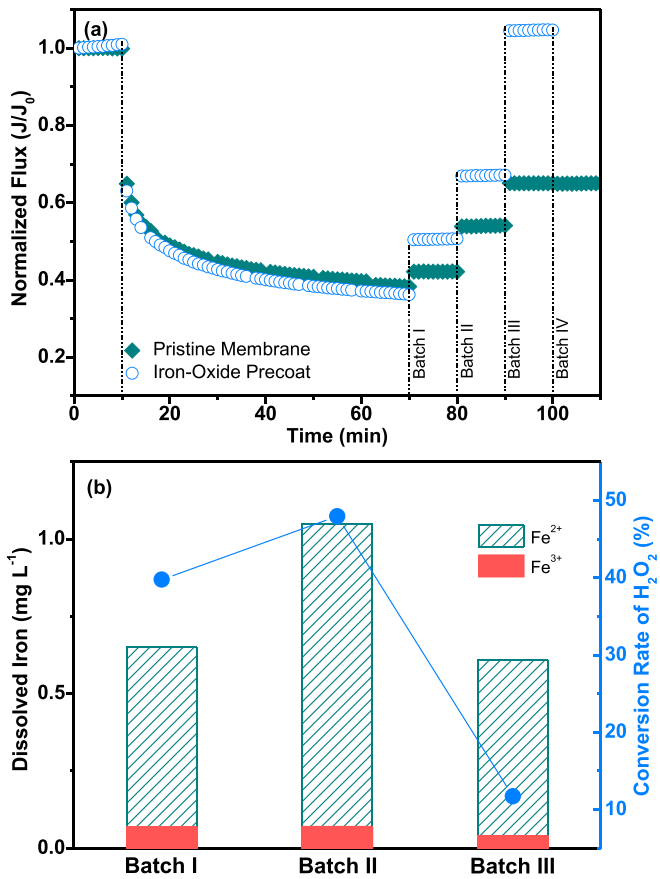

Fig. 4. (a) Batch cleaning of pristine and iron-oxide pre-coated membranes with single H_2O_2 ($[H_2O_2]_0$ = 30.0 mM, pH = 2.5). (b) Iron leaching and H_2O_2 conversion during H_2O_2 cleaning of iron-oxide pre-coated membrane.

partial pore narrowing/plugging by alginate branches [38]. Afterwards, a slower decrease of the permeate flux was observed, until the end of filtration, likely attributing to gradual formation of a cake layer [39]. The evident flux decline during the fouling processes indicated that the fluxes applied in the experiments should be beyond the critical flux [40]. Subsequently, the fouled iron-oxide pre-coated and pristine membranes were, respectively, subjected to three and four batches (20 h for each batch) of H_2O_2 cleaning (30.0 mM, pH 2.5). The demineralized water flux of the pristine membrane was slowly restored during three consecutive cleaning batches until a flux recovery of 43.29%, presumably owing to direct oxidation by H_2O_2 of low oxidation power (reduction potential ($E^\circ H_2O_2/H_2O$) = 1.763 V) [41]. After the third cleaning batch, the flux reached a plateau, manifesting that the remaining alginate residues on the membrane surface were resistant to the direct oxidation by H_2O_2. However, the flux recovery of the iron-oxide pre-coated membrane in each cleaning batch was much higher than that of the membrane without pre-coat, likely ascribed to the high oxidation power of $^\bullet OH$ (E° $^\bullet OH$, H^+/H_2O = 2.730 ± 0.017 V) generated by Fe_3O_4-initiated Fenton reactions [42]. After the third cleaning batch, the flux appeared even slightly higher than its initial level, which was likely caused by partial loss of Fe_3O_4 layer from the membrane surface because of the long cleaning process with H_2O_2 solutions.

To verify the contribution of Fenton-based processes to membrane cleaning, iron leaching and H_2O_2 conversion were simultaneously monitored. As depicted in Fig. 4b, during each batch cleaning of the iron-oxide pre-coated membrane, Fe(II) ions (0.6–1.0 mg L^{-1}) were detected as the dominant iron species leached from the Fe_3O_4 layer, and a decrease of H_2O_2 concentration (by 12–48%) was also observed. Typically, the dissolved Fe(II) would instantaneously react with H_2O_2 through homogenous Fenton reactions to generate $^\bullet OH$ radicals (Eq. (3), $k = 63\ M^{-1}\ s^{-1}$) [43]. However, due to the overdose of H_2O_2 relative to the dissolved Fe(II) ($[H_2O_2]$:[Fe(II)] = 30/0.01 mM/mM), the produced free $^\bullet OH$ in the aqueous phase inclined to be scavenged by the excessive H_2O_2 (Eq. (4), $k = 2.7 \times 10^7\ M^{-1}\ s^{-1}$), instead of degrading membrane foulants [44]. By comparing the reaction rates of Eq. (5) and Eq. (6), the Fe(II), prevailing in the bulk solution, should originate from the $HO_2^\bullet$-governed reduction of Fe(III) (Eq. (6), $k = 2 \times 10^3\ M^{-1}\ s^{-1}$) rather than from the Fe(III) reduction by H_2O_2 (Eq. (5), $k = 2.7 \times 10^{-3}\ M^{-1}\ s^{-1}$) [44,45]. These results suggested that homogeneous Fenton reactions of H_2O_2 with Fe(II) (or Fe(III)) did not play an important role in $^\bullet OH$ generation for the oxidative cleaning.

$$Fe(II) + H_2O_2 + H^+ \rightarrow Fe(III) + {}^\bullet OH + H_2O \quad (3)$$

$$H_2O_2 + {}^\bullet OH \rightarrow H_2O + HO_2^\bullet \quad (4)$$

$$Fe(III) + H_2O_2 \rightarrow Fe(II) + HO_2^\bullet + H^+ \quad (5)$$

$$Fe(III) + HO_2^\bullet \rightarrow Fe(II) + O_2 + H^+ \quad (6)$$

Therefore, in the H_2O_2 cleaning, the foulant decay presumably proceeded through heterogeneous Fenton processes, catalysed by the Fe_3O_4 surface. Regarding this, Lin and Gurol proposed the reaction routes of H_2O_2 decomposition on iron oxide surfaces (Eq. (7)–(11)) [46]:

$$\equiv Fe(II) - OH + H_2O_2 \rightarrow \equiv Fe(III) - OH + {}^\bullet OH \quad (7)$$

$$\equiv Fe(III) - OH + H_2O_2 \rightarrow (H_2O_2)_{ads} \quad (8)$$

$$(H_2O_2)_{ads} \rightarrow \equiv Fe(II) + H_2O + HO_2^\bullet \quad (9)$$

$$HO_2^\bullet \leftrightarrow H^+ + O_2^{\bullet -}\ (pKa = 4.8) \quad (10)$$

$$\equiv Fe(III) - OH + HO_2^\bullet \rightarrow \equiv Fe(II) + H_2O + O_2 \quad (11)$$

Herein, the heterogeneous Fenton reactions took place at the Fe_3O_4-foulant interface, where the iron-oxide catalysts, foulants and H_2O_2 coexisted. The H_2O_2 surface reactions and $^\bullet OH$ formation at the Fe_3O_4-foulant interface were then favourable for the oxidative detachment of the fouling layer from the membrane surface [47]. Prior to the surface reactions, H_2O_2 should be diffusively transported from the bulk solution to the Fe_3O_4-foulant interface, where it was supposed to react with the Fe_3O_4 layer. Therefore, it could be anticipated that the limited H_2O_2 penetration into the Fe_3O_4-foulant interface inclined to prolong the time that was needed for cleaning the iron-oxide pre-coated membrane, attributing to the H_2O_2 diffusion barrier caused by the compact fouling layer [48].

3.4. Oxalic acid-aided Fenton cleaning of iron-oxide pre-coated membranes

As depicted in Fig. 5a, the permeate fluxes of pristine membranes were poorly restored (by 5.81% or 7.96%, respectively) by sole oxalic acid (11.1 mM) or binary oxalic acid/H_2O_2 (11.1 mM, 30.0 mM) cleaning. Without a Fe_3O_4 catalytic layer, the slight flux recoveries were likely attributed to fouling layer relaxation by oxalic acid or weak oxidation by H_2O_2. Owing to the higher stability constant of Ca^{2+}-oxalate ($\log\beta$ = 3.0–3.4) than that of Ca^{2+}-alginate ($\log\beta$ = 2.2), oxalic acid should be capable of extracting the Ca^{2+} out of the cross-linked Ca^{2+}-alginate matrix and loosening its compact configuration [49,50]. Meanwhile, the water fluxes of the oxalic acid (or oxalic acid/H_2O_2) treated pristine membranes nearly decreased to their before-cleaning levels after Ca^{2+} exposure (3.0 mM). This result signified that in the non-oxidative cleaning system, some foulants, loosened by oxalic acid, still persisted on the membrane surface or in the membrane pores, and tended to be re-organised into a cross-linked conformation through complexing with Ca^{2+} [51]. As observed in Fig. 5b, oxalic acid cleaning

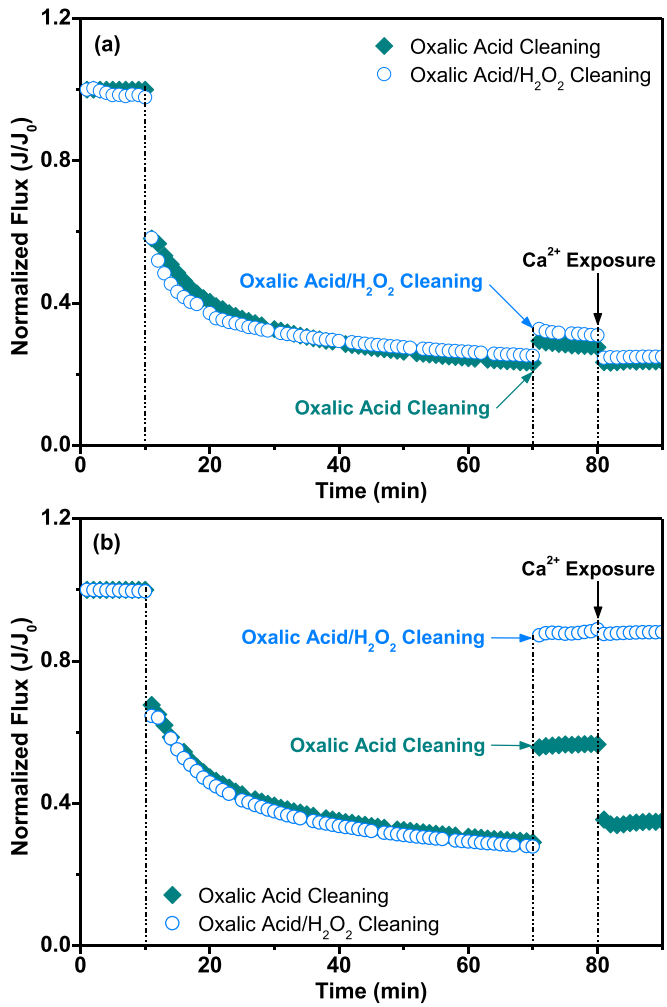

Fig. 5. Cleaning of (a) pristine and (b) iron-oxide pre-coated membranes with single oxalic acid and oxalic acid/H_2O_2 combination ([oxalic acid]$_0$ = 11.1 mM, [H_2O_2]$_0$ = 30.0 mM, pH = 2.5). The Ca^{2+} exposure tests were conducted at [Ca^{2+}]$_0$ = 3.0 mM and pH = 7.0.

resulted in a higher flux recovery (38.73%) for the iron-oxide pre-coated membrane, presumably because the oxalic acid could dissolve some Fe_3O_4 (leached Fe_T: 43.31%, 4.46 mg L^{-1}, Table 1), and then partially detached the Ca^{2+}-alginate layer. The flux also encountered a decline (by 78.07%) after Ca^{2+} exposure, further confirming that the remaining gel layer was re-compacted upon exposure to Ca^{2+}. Notably, the flux was recovered by 85.07% when combining H_2O_2 and oxalic acid for cleaning the iron-oxide pre-coated membrane and no flux decrease was observed upon Ca^{2+} exposure. This result suggested that the gel-like fouling layer was sufficiently removed from the iron-oxide pre-coat by the synergistic cleaning of oxalic acid relaxation and Fenton oxidation. Herein, the surface $^{\bullet}OH$ radicals were expected to preferentially attack the alginate molecules without evident scavenging by oxalic acid, due to the much lower reaction rate of $^{\bullet}OH$/oxalic acid ($k_{\bullet OH/oxalic\ acid} = 1.4 \times 10^6\ M^{-1}\ s^{-1}$) than that of $^{\bullet}OH$/alginate ($k_{\bullet OH/alginate} = 9.2 \times 10^7\ M^{-1}\ s^{-1}$) [52, 53]. In comparison with the Fenton cleaning without using oxalic acid (Section 3.3), the synergistic oxalic acid/H_2O_2 cleaning of the iron-oxide pre-coated membrane consumed much less H_2O_2 (9.6%, Table 1) and shorter cleaning time (1 h), which was presumably attributable to an accelerated diffusion of H_2O_2 to the Fe_3O_4/foulant interface due to gel layer relaxation by oxalic acid.

Practicality of the synergistic oxalic acid/H_2O_2 cleaning was evaluated via multicycle filtration/cleaning with the iron-oxide pre-coated membrane (Fig. 6a). Each cycle included filtration of Ca^{2+}-alginate solution (0.8 g L^{-1}) for 1 h, followed by oxalic acid/H_2O_2 (11.1 mM/30.0

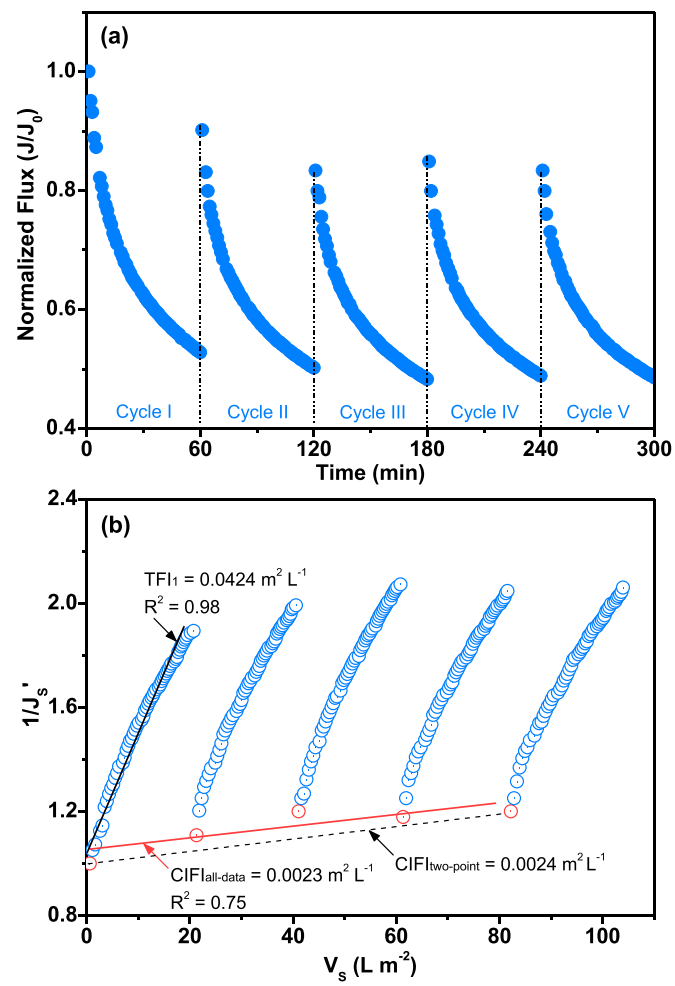

Fig. 6. (a) Multicycle filtration/cleaning of iron-oxide pre-coated membrane by oxalic acid/H_2O_2 combination ([oxalic acid]$_0$ = 11.1 mM, [H_2O_2]$_0$ = 30.0 mM, pH = 2.5). (b) Evaluation of total fouling indices (TFI) and chemically irreversible fouling indices (CIFI). The iron-oxide pre-coat was not refreshed between the cycles.

Table 1
Comparison of cleaning performance between iron-oxide precoated and pristine ceramic nanofiltration membranes fouled with Ca^{2+}-alginate gel layer (ND: not detected).

Membranes	Foulants	Cleaning agents	Dissolved Fe^{2+} (mg L^{-1})	Dissolved Fe^{3+} (mg L^{-1})	H_2O_2 conversion (%)	Flux recovery (%)
Iron-oxide precoat	Ca^{2+}-alginate	Oxalic acid/H_2O_2	ND	0.66	9.6	85.07
Iron-oxide precoat	Ca^{2+}-alginate	H_2O_2	ND	ND	0	7.80
Iron-oxide precoat	Ca^{2+}-alginate	Oxalic acid	0.25	4.21	–	38.73
Pristine membrane	Ca^{2+}-alginate	Oxalic acid/H_2O_2	–	–	0	7.96
Pristine membrane	Ca^{2+}-alginate	H_2O_2	–	–	0	6.31
Pristine membrane	Ca^{2+}-alginate	Oxalic acid	–	–	–	5.81

mM) cleaning for 15 min. The iron-oxide pre-coat was not refreshed between the cycles. Within the first three cycles of oxalic acid/H_2O_2 cleaning, over 90% of the initial flux was maintained, and then the initial flux decreased to ~83%. After the third cleaning, the initial normalized flux of the membrane reached a plateau level of 83–85%. These results implied that most of the gel-like foulants could be reversed from the iron-oxide pre-coated membrane by the synergistic oxalic acid/H_2O_2 cleaning, while some irreversible fouling might occur at the early stage (i.e., the first three cycles) of the multicycle filtration/cleaning [22]. The slightly higher initial normalized flux (84.9%) after the third cleaning, than that after the second cleaning (83.3%), was possibly resulted from a partial falling-off of the Fe_3O_4 layer from the membrane, which might release some blocked pores for water permeation. Kramer et al. reported that hydraulic backwash could recover the permeability of gel-fouled ceramic NF membranes maximally by 43% but damaged the membrane integrity, and forward flush slightly restored the permeability (<10%) [54]. This indicated that the synergistic cleaning method of this work might be a promising substitute for conventional hydraulic backwash and forward flush for cleaning ceramic NF membranes. As depicted in Fig. S1, approximately 26.5% of the Fe_3O_4 nanoparticles were leached after five cleaning cycles, probably due to the hydraulic scouring and chemical leaching during the oxalic acid/H_2O_2 circulation. As suggested by Pan et al. [55], the remaining iron-oxide layer (~2.1 μm in thickness, Fig. 7a) after five filtration/cleaning cycles was likely ascribed to the drag forces caused by radial flow, frictional forces and molecular forces between the particles. Furthermore, the iron layer still presented a homogeneous and dense coating on the membrane surface (Fig. 7b), which could provide sufficient active sites for Fenton-based reactions. Additionally, as shown in Fig. 7c, the XRD patterns of the iron-oxide pre-coated membrane

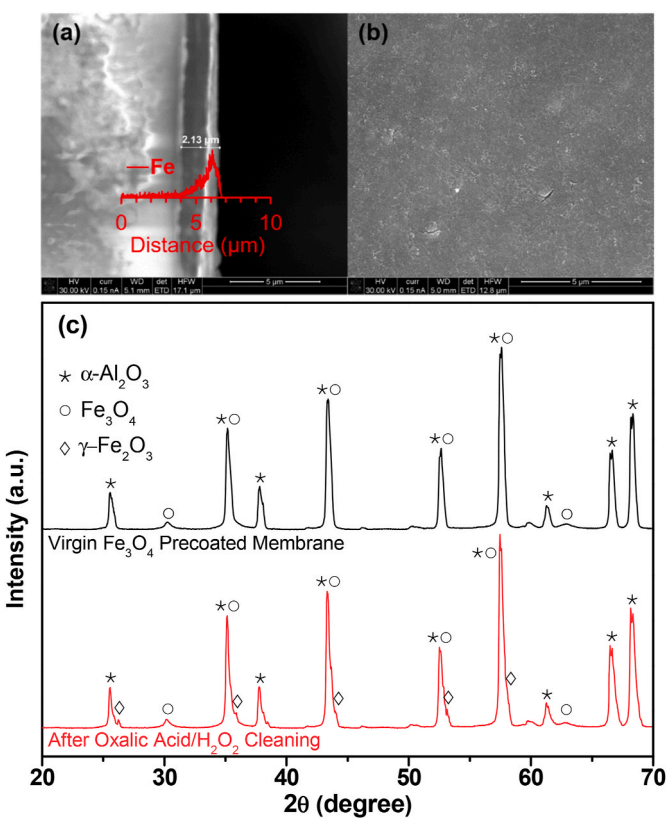

Fig. 7. (a) Cross-section SEM image with inset EDS profile and (b) top-view SEM image of iron-oxide pre-coated membrane after five cycles of Ca^{2+}-alginate filtration and oxalic acid/H_2O_2 cleaning. (c) XRD patterns of iron-oxide pre-coated membrane before and after five cycles of Ca^{2+}-alginate filtration and oxalic acid/H_2O_2 cleaning.

corresponded to the cubic spinel structure of Fe_3O_4, signifying an abundance of active Fe_3O_4 species on the membrane surface [56]. After multicycle filtration/cleaning, the characteristic peaks of the Fe_3O_4 nanoparticles were almost unchanged except for a presence of reflection peaks of γ-Fe_2O_3 (maghemite), indicating a partial conversion of the Fe_3O_4 to the γ-Fe_2O_3 phase after oxidation reactions [56]. The XRD profiles showed an evident α-Al_2O_3 crystalline phase of the Al_2O_3 supporting layer, but no apparent characteristic peaks of TiO_2 and ZrO_2 were observed, which indicated an amorphous structure of the TiO_2 active layer and ZrO_2 inter-layer [57].

To predict the long-term performance of using oxalic acid-assisted Fenton oxidation for cleaning iron-oxide pre-coated membrane, the fouling reversibility, developed in the multicycle filtration/cleaning, was quantitatively studied through a statistical analysis of the unified membrane fouling index (*UMFI*) values. As observed in Fig. 6b, the regression-line slopes of the cyclic fouling curves from Eq. (2) [32] corresponded to total fouling index (*TFI*) values of five filtration cycles, varying in a range of 3.51×10^{-2} to 4.24×10^{-2} $m^2 L^{-1}$ (averaging 3.94×10^{-2} $m^2 L^{-1}$, $R^2 \geq 0.98$). These values were much higher than the *TFI* value (1.13×10^{-3} m^2 L^{-1}) in ceramic UF membrane fouling by Ca^{2+}-alginate as reported by Alresheedi et al., suggesting a faster fouling tendency of the ceramic NF membrane by gel-like foulants compared to the ceramic UF membrane [58]. The chemically irreversible fouling index (*CIFIall-data*) value was 2.3×10^{-3} $m^2 L^{-1}$, as represented by the slope of the regression-line connecting the starting points of the five fouling curves ($R^2 = 0.75$), which was comparable to the *CIFItwo-point* (2.4×10^{-3} $m^2 L^{-1}$) determined by the two-point approach [32]. The chemically irreversible fouling ratio (*CIFI/TFI* = 5.8%) in the oxalic acid/H_2O_2 cleaning (15 min) was much lower than those (20% and 38%, respectively) in NaOH (10 mM) and NaClO (14 mM) cleaning with even longer duration (4 h), indicating a higher efficiency and reversibility of using oxalic acid-aided Fenton oxidation for cleaning gel-like fouling, compared to the conventional NaOH and NaClO cleaning [58].

3.5. Iron leaching of iron-oxide pre-coated membranes

The combined use of iron-oxide pre-coat and oxalic acid favoured iron leaching, as observed in Fig. 8. This could be potentially attributed to three underlying mechanisms, such as protonation, non-reductive complexation and reductive dissolution [59]. Herein, the protonation and reductive dissolution were excluded to be the possible causes for the iron dissolution, due to the negligible pH variation (pH = 2.5–2.6, Fig. S2) during Fe_3O_4/oxalic acid (or Fe_3O_4/oxalic acid-H_2O_2) interactions and minimal Fe(II) generation after the oxalic acid or oxalic acid/H_2O_2 treatment (Fe(II) ≤ 0.25 mg L^{-1}, Table 1). Non-reductive complexation of Fe_3O_4/oxalic acid was thus supposed to act as the dominant pathway for the iron leaching from the iron-oxide pre-coat surface [60]. The comparison of the iron leaching from the iron-oxide pre-coat by oxalic acid (11.0 mM) and oxalic acid/H_2O_2 (11.0/30.0 mM) in the presence and absence of Ca^{2+}-alginate fouling layer is illustrated in Fig. 8a. The iron leaching of the bare iron-oxide pre-coat by oxalic acid could be described as a linear function of time ($Fe_T = 0.8664\ t$, $R^2 = 0.99$). This result suggested that the Fe leaching of the iron-oxide pre-coat by oxalic acid was possibly governed by slow ionization of the oxalic acid ($pKa_1 = 1.25$, $pKa_2 = 4.27$), which constantly supplied dissociated oxalic acid for iron dissolution [61]. Additionally, the maximal Fe leaching (13.4%) of the iron-oxide pre-coat by oxalic acid/H_2O_2 combination appeared much lower than that caused by oxalic acid (50.8%) within an identical time scale (60 min), which indicated a potential inhibition of iron dissolution by H_2O_2 addition into oxalic acid solutions [62].

As suggested by Xue et al. [53], the dissolution of Fe_3O_4 via complexation is a surface-controlled reaction occurring in two steps, adsorption of ligand on oxide surfaces through ligand exchange and iron dissolution by weakening Fe–O bonds of Fe_3O_4. To elucidate the inhibiting effect of H_2O_2 on the oxalic acid-induced iron leaching of the

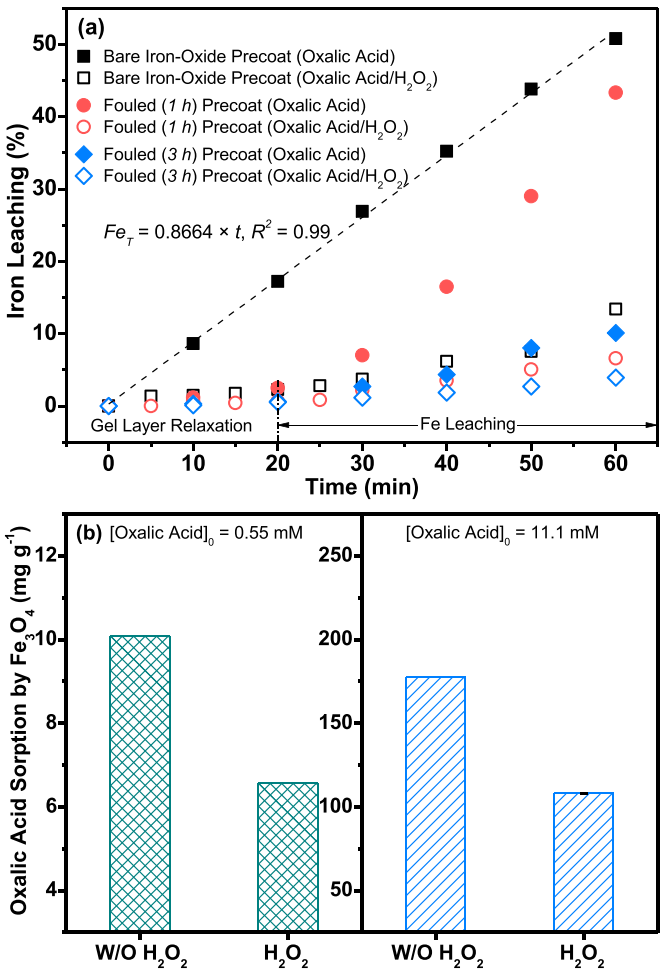

Fig. 8. (a) Iron leaching of bare and fouled iron-oxide pre-coat by single oxalic acid and oxalic acid/H_2O_2 combination ([oxalic acid]$_0$ = 11.1 mM, [H_2O_2]$_0$ = 30.0 mM, pH = 2.5). (b) Oxalic acid sorption by Fe_3O_4 powders with and without (W/O) addition of H_2O_2 ([Fe_3O_4]$_0$ = 1.0 g L^{-1}, [H_2O_2]$_0$ = 30.0 mM, pH = 2.5).

iron-oxide pre-coat, the surface adsorption of oxalic acid on Fe_3O_4 colloids was investigated with batch adsorption tests in the presence and absence of H_2O_2. As depicted in Fig. 8b, the adsorption of oxalic acid ([oxalic acid]$_0$ = 0.55 mM) by the Fe_3O_4 colloids was markedly decreased by 34.9% by H_2O_2 addition into the Fe_3O_4/oxalic acid matrix, even a greater inhibition (by 39.1%) by H_2O_2 on the oxalic acid adsorption could be observed for the oxalic acid of higher initial concentration (11.1 mM). Moreover, since the free oxalic acid remaining in the solution was increased after the H_2O_2 addition (Fig. S3), most of the oxalic acid was thus supposed not to be degraded by Fenton-based oxidation but remained in the aqueous phase or on the Fe_3O_4 surface [26]. Therefore, the decreased iron-leaching of the iron-oxide pre-coat in the oxalic acid/H_2O_2 matrix was presumably not attributable to potential degradation of oxalic acid in the presence of H_2O_2, but to an underlying adsorptive competition between H_2O_2 and oxalic acid on the Fe_3O_4 surface, which was also found by Rodríguez et al. [62].

Compared with the bare iron-oxide pre-coat, the Ca^{2+}-alginate fouled (for 1 h) membane underwent firstly a minimal Fe dissolution (Fe_T leaching: 2.47%) by oxalic acid at the early stage (20 min), but developed an exponential increase at the later stage (Fe_T leaching: 43.31%) (Fig. 8a). The nonlinear two-stage profile of leached Fe_T vs. time suggested that the iron leaching rate of the fouled iron-oxide pre-coat was not entirely surface-reaction limited, but also relied on transport-controlled steps, such as oxalic acid diffusion through the gel layer [47]. As such, it could be inferred that the Ca^{2+}-alginate gel layer as a steric barrier supressed the iron leaching at an early stage, but inclined to be loosened by oxalic acid following continuous oxalic acid/-Ca^{2+}-alginate complexation, which in turn promoted the diffusion of oxalic acid onto the Fe_3O_4 surface [63]. Hence, during the 15-min oxalic acid/H_2O_2 cleaning in the multicycle filtration/cleaning (Section 3.4), the compact gel-like cake layer, formed on the iron-oxide pre-coat, made that the hydraulic scouring could not directly act on the iron-oxide pre-coat surface, which protected the iron layer from being flushed away by cross flow to some extent. Likewise, the introduction of H_2O_2 restricted the Fe leaching by oxalic acid (by 84.8%), likely due to a promoted diffusion and competitive adsorption of H_2O_2 onto the iron-oxide pre-coat surface. This result well accounted for the desirable stability and reproducibility of the iron-oxide pre-coat during multicycle runs of oxalic acid-aided Fenton cleaning, as discussed in Section 3.4. A two-stage leaching of iron, but to a less extent (Fe_T leaching: 10.1% by oxalic acid, 3.9% by oxalic acid/H_2O_2), could also be observed with a more severely fouled (for 3 h) iron-oxide pre-coat. The findings of the oxalic acid/H_2O_2 cleaning (Section 3.4, Fig. 5) and the iron leaching experiments (Fig. 8) demonstrated an underlying synergistic effect between oxalic acid and H_2O_2, regarding the gel layer relaxation/oxidation and Fe-leaching suppression, for effective defouling of iron-oxide pre-coated ceramic NF membranes, which can be illustrated by Scheme 1.

3.6. Implications for the direct treatment of surface water

Filtration of canal water for 5 d was performed using a Fe_3O_4 pre-coated ceramic NF membrane, with 15-min oxalic acid/H_2O_2 cleaning every 24 h. The relative production downtime during membrane cleaning was 0.62 min h^{-1}, much lower than the value (2.6 min h^{-1}) of NaClO cleaning for ceramic NF membranes reported by Kramer et al. [2]. The iron-oxide pre-coat (pre-coated for 30 min) was reused over the five cycles (5 d) of canal water filtration, which would presumably exert an insignificant impact on the continuous operations of the pre-coated membranes in practice. As depicted in Fig. S4a, a fast drop of permeability (~38.7%) was also observed in the NF processes of the canal water, when switching the pure water filtration to the canal water filtration, which was similar to the phenomenon found in the NF with alginate (Fig. 4a). The membrane permeability with canal water decreased by 48.7% in the first cycle, indicating the high fouling potential of the canal water towards the membrane. The initial canal-water permeability for the following cycles were recovered to ~90% after oxalic acid/H_2O_2 cleaning, implying high cleaning efficiencies during the long-term filtration with canal water. During the five cycles, the oxalic acid/H_2O_2 solution was reused, which reduced the consumption of chemicals and production of oxalic acid wastewater. As mentioned by earlier studies, oxalic acid could be well degraded in aerobic conditions with microbial treatment technologies (i.e., activated sludge), a normal aerobic wastewater treatment plant could thus deal with the produced oxalic acid wastewater [64]. Furthermore, Table S2 presents that the iron-oxide pre-coated membrane rejected ~90% of DOC and UV_{254}, suggesting its high rejection of organic matter probably owing to steric exclusion by the ceramic NF membrane. By contrast, the rejection rates of anions and cations appeared to be much lower, which were 43–78% and 27–42%, respectively. Notably, after the five cycles (5 d) of filtration/cleaning, there still was a certain amount of iron-oxide pre-coat (~0.9 μm in thickness, Fig. S4b) remaining on the membrane surface, indicating a potential applicability of using iron-oxide pre-coated NF membranes for long-term water treatment.

3.7. Research needs and challenges

The cleaning strategy, proposed in this work, provides a pathway of using pressure-driven pre-filtration of Fe_3O_4 nanoparticles to obtain a catalytic ceramic NF system for fouling control in water treatment.

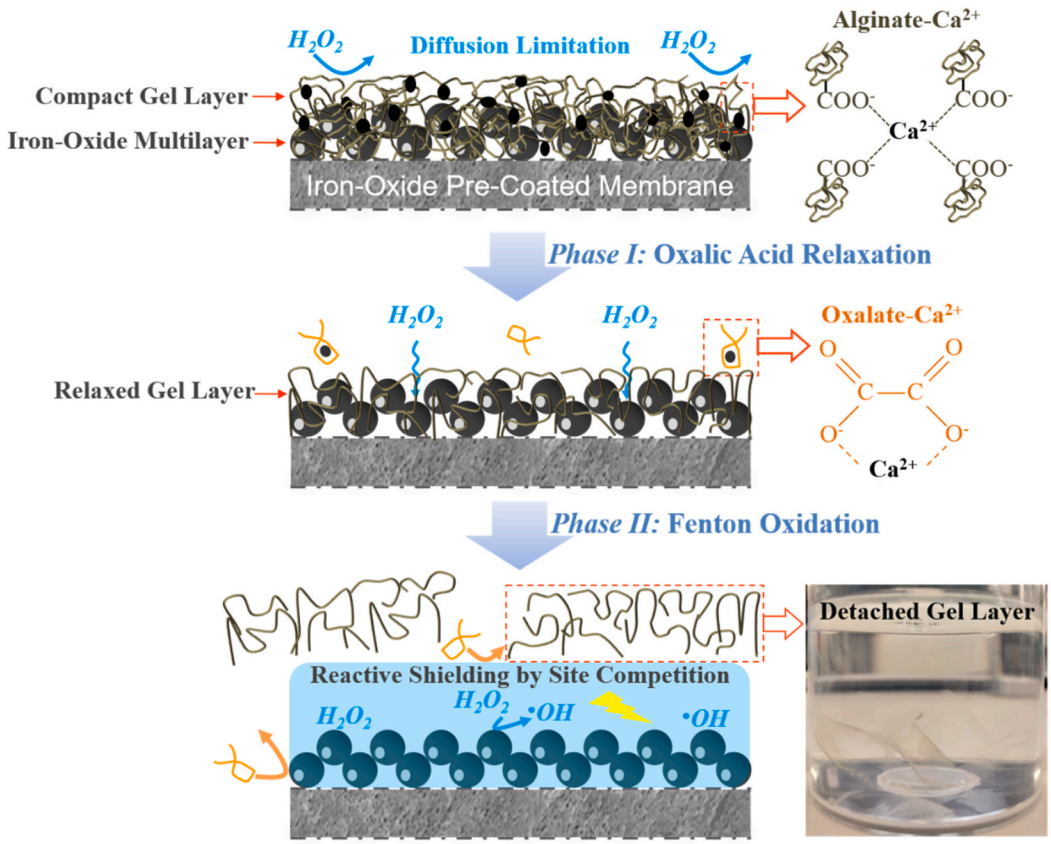

Scheme 1. Mechanism illustration of synergistic effect between oxalic acid and H_2O_2 for cleaning iron-oxide pre-coated membrane fouled with Ca^{2+}-mediated gel layer and protective effect of H_2O_2 on iron-oxide pre-coat.

However, the long-term usage of Fe_3O_4-pre-coated ceramic NF membrane in industries may be limited by the stability and reactivity of catalyst pre-coat. Further studies on using stable and active catalysts for improving the pre-coated catalytic ceramic membrane are thus needed. Additionally, as can be speculated from this study, the synergistic relaxation-oxidation method, currently tested as a proof of principle, may apply to other types of Ca^{2+}-mediated fouling (i.e., humic acids) due to their similar mechanisms in the formation of a gel layer on membrane surfaces via Ca^{2+} bridging [20]. We thus believe that understanding the roles of oxalic acid and Fenton-based oxidation in the typical Ca^{2+}-mediated alginate fouling, may provide insights into handling other Ca^{2+}-derived fouling with an integration of chelation/oxidation. However, the integrative method should be further piloted in practice and explored for more complex real water matrices, also to understand how other compounds could interfere.

4. Conclusions

In this work, a synergistic method of coupling oxalic acid chelation and Fe_3O_4-activated Fenton oxidation process was proposed for cleaning persistent gel-like fouling of ceramic NF membrane. The conclusions can be drawn as follows:

Cross-flow pre-filtration of Fe_3O_4 nanoparticles was able to pre-coat a uniform reproducible iron-oxide layer on top of the ceramic NF membrane. The pre-coat thickness was controlled by the *trans*-membrane pressure (2.0–10.0 bar), only causing a minimal decrease of membrane permeability (<10%).

Synergistic effect between oxalic acid relaxation and Fenton-based oxidation processes played a key role in the removal of gel layer, which was presumably attributed to enhanced diffusive transport of H_2O_2 at the iron-oxide pre-coat/foulant interface.

Oxalic acid-aided Fenton cleaning for 15 min achieved stable initial normalized fluxes (83.33–90.15%) of the iron-oxide pre-coated membrane during five filtration/cleaning cycles, with no need of refreshing the iron-oxide pre-coat between the cycles. The leaching of iron from the iron-oxide pre-coat was suppressed in the oxalic acid/H_2O_2 matrix, which was likely due to a reactive shielding by competitive reactions of H_2O_2 on the Fe_3O_4 surface.

Declaration of competing interest

The authors declare that they have no known competing financial interests or personal relationships that could have appeared to influence the work reported in this paper.

Acknowledgement

The authors acknowledge the PhD scholarship awarded to Bin Lin (No. 201706190224) by the China Scholarship Council, China.

Appendix A. Supplementary data

Supplementary data to this article can be found online at https://doi.org/10.1016/j.memsci.2021.119553.

Author statement

Bin Lin: Conceptualization, Methodology, Investigation, Data curation, Writing - original draft. Sebastiaan G.J. Heijman: Conceptualization, Methodology, Writing - review & editing, Supervision. Ran Shang: Methodology. Luuk C. Rietveld: Writing - review & editing, Supervision.

References

[1] T. Fujioka, S.J. Khan, J.A. McDonald, L.D. Nghiem, Nanofiltration of trace organic chemicals: a comparison between ceramic and polymeric membranes, Separ. Purif. Technol. 136 (2014) 258–264, https://doi.org/10.1016/j.seppur.2014.08.039.

[2] F.C. Kramer, R. Shang, S.G.J. Heijman, S.M. Scherrenberg, J.B. van Lier, L. C. Rietveld, Direct water reclamation from sewage using ceramic tight ultra- and nanofiltration, Separ. Purif. Technol. 147 (2015) 329–336, https://doi.org/10.1016/j.seppur.2015.04.008.

[3] X.-M. Wang, T.D. Waite, Gel layer formation and hollow fiber membrane filterability of polysaccharide dispersions, J. Membr. Sci. 322 (2008) 204–213, https://doi.org/10.1016/j.memsci.2008.05.033.

[4] Y.-Y. Zhao, X.-M. Wang, H.-W. Yang, Y.-F.F. Xie, Effects of organic fouling and cleaning on the retention of pharmaceutically active compounds by ceramic nanofiltration membranes, J. Membr. Sci. 563 (2018) 734–742, https://doi.org/10.1016/j.memsci.2018.06.047.

[5] M. Zhang, H. Lin, L. Shen, B.-Q. Liao, X. Wu, R. Li, Effect of calcium ions on fouling properties of alginate solution and its mechanisms, J. Membr. Sci. 525 (2017) 320–329, https://doi.org/10.1016/j.memsci.2016.12.006.

[6] Y. Xin, M.W. Bligh, A.S. Kinsela, Y. Wang, T. David Waite, Calcium-mediated polysaccharide gel formation and breakage: impact on membrane foulant hydraulic properties, J. Membr. Sci. 475 (2015) 395–405, https://doi.org/10.1016/j.memsci.2014.10.033.

[7] Y. Xin, M.W. Bligh, A.S. Kinsela, T.D. Waite, Effect of iron on membrane fouling by alginate in the absence and presence of calcium, J. Membr. Sci. 497 (2016) 289–299, https://doi.org/10.1016/j.memsci.2015.09.023.

[8] G. Mustafa, K. Wyns, P. Vandezande, A. Buekenhoudt, V. Meynen, Novel grafting method efficiently decreases irreversible fouling of ceramic nanofiltration membranes, J. Membr. Sci. 470 (2014) 369–377, https://doi.org/10.1016/j.memsci.2014.07.050.

[9] T. Fujioka, A.T. Hoang, T. Okuda, H. Takeuchi, H. Tanaka, L.D. Nghiem, Water reclamation using a ceramic nanofiltration membrane and surface flushing with ozonated water, Int. J. Environ. Res. Publ. Health 15 (2018), https://doi.org/10.3390/ijerph15040799.

[10] S.S. Wadekar, R.D. Vidic, Comparison of ceramic and polymeric nanofiltration membranes for treatment of abandoned coal mine drainage, Desalination 440 (2018) 135–145, https://doi.org/10.1016/j.desal.2018.01.008.

[11] P. van den Brink, A. Zwijnenburg, G. Smith, H. Temmink, M. van Loosdrecht, Effect of free calcium concentration and ionic strength on alginate fouling in cross-flow membrane filtration, J. Membr. Sci. 345 (2009) 207–216, https://doi.org/10.1016/j.memsci.2009.08.046.

[12] M.S. Mauter, I. Zucker, F. Perreault, J.R. Werber, J.-H. Kim, M. Elimelech, The role of nanotechnology in tackling global water challenges, Nat. Sustain. 1 (2018) 166–175, https://doi.org/10.1038/s41893-018-0046-8.

[13] X.-J. Yang, X.-M. Xu, X.-C. Xu, J. Xu, H.-L. Wang, R. Semiat, Y.-F. Han, Modeling and kinetics study of Bisphenol A (BPA) degradation over an $FeOCl/SiO_2$ Fenton-like catalyst, Catal. Today 276 (2016) 85–96, https://doi.org/10.1016/j.cattod.2016.01.002.

[14] L. De Angelis, M.M.F. de Cortalezzi, Improved membrane flux recovery by Fenton-type reactions, J. Membr. Sci. 500 (2016) 255–264, https://doi.org/10.1016/j.memsci.2015.11.042.

[15] S. Sun, H. Yao, W. Fu, L. Hua, G. Zhang, W. Zhang, Reactive photo-Fenton ceramic membranes: synthesis, characterization and antifouling performance, Water Res. 144 (2018) 690–698, https://doi.org/10.1016/j.watres.2018.08.002.

[16] J. Zhang, X.-L. Jiao, Y.-G. Xia, F.-F. Liu, Y.-P. Pang, X.-F. Zhao, D.-R. Chen, Enhanced catalytic activity in liquid-exfoliated FeOCl nanosheets as a fenton-like catalyst, Chem. Eur J. 22 (2016) 9321–9329, https://doi.org/10.1002/chem.201600172.

[17] Z. Zhou, X. He, M. Zhou, F. Meng, Chemically induced alterations in the characteristics of fouling-causing bio-macromolecules – implications for the chemical cleaning of fouled membranes, Water Res. 108 (2017) 115–123, https://doi.org/10.1016/j.watres.2016.10.065.

[18] S. Li, S.G.J. Heijman, J.Q.J.C. Verberk, A.R.D. Verliefde, A.J.B. Kemperman, J. C. van Dijk, G. Amy, Impact of backwash water composition on ultrafiltration fouling control, J. Membr. Sci. 344 (2009) 17–25, https://doi.org/10.1016/j.memsci.2009.07.025.

[19] J. Chen, M. Zhang, F. Li, L. Qian, H. Lin, L. Yang, X. Wu, X. Zhou, Y. He, B.-Q. Liao, Membrane fouling in a membrane bioreactor: high filtration resistance of gel layer and its underlying mechanism, Water Res. 102 (2016) 82–89, https://doi.org/10.1016/j.watres.2016.06.028.

[20] Q. Li, M. Elimelech, Organic fouling and chemical cleaning of nanofiltration membranes: Measurements and mechanisms, Environ. Sci. Technol. 38 (2004) 4683–4693, https://doi.org/10.1021/es0354162.

[21] W. Song, V. Ravindran, B.E. Koel, M. Pirbazari, Nanofiltration of natural organic matter with H_2O_2/UV pretreatment: fouling mitigation and membrane surface characterization, J. Membr. Sci. 241 (2004) 143–160, https://doi.org/10.1016/j.memsci.2004.04.034.

[22] C.P. Athanasekou, S.K. Papageorgiou, V. Kaselouri, F.K. Katsaros, N.K. Kakizis, A. A. Sapalidis, N.K. Kanellopoulos, Development of hybrid alginate/ceramic membranes for Cd^{2+} removal, Microporous Mesoporous Mater. 120 (2009) 154–164, https://doi.org/10.1016/j.micromeso.2008.07.048.

[23] D. Lu, T. Zhang, L. Gutierrez, J. Ma, J.-P. Croué, Influence of surface properties of filtration-layer metal oxide on ceramic membrane fouling during ultrafiltration of oil/water emulsion, Environ. Sci. Technol. 50 (2016) 4668–4674, https://doi.org/10.1021/acs.est.5b04151.

[24] B.-C. Kim, J.-W. Nam, K.-H. Kang, Dynamic membrane filtration using powdered iron oxide for SWRO pre-treatment during red tide event, J. Membr. Sci. 524 (2017) 604–611, https://doi.org/10.1016/j.memsci.2016.11.081.

[25] J.F. Soesanto, K.-J. Hwang, C.-W. Cheng, H.-Y. Tsai, A. Huang, C.-H. Chen, T.-W. Cheng, K.-L. Tung, Fenton oxidation-based cleaning technology for powdered activated carbon-precoated dynamic membranes used in microfiltration seawater pretreatment systems, J. Membr. Sci. 591 (2019) 117298, https://doi.org/10.1016/j.memsci.2019.117298.

[26] E. Rodríguez, G. Fernández, B. Ledesma, P. Álvarez, F.J. Beltrán, Photocatalytic degradation of organics in water in the presence of iron oxides: influence of carboxylic acids, Appl. Catal. B Environ. 92 (2009) 240–249, https://doi.org/10.1016/j.apcatb.2009.07.013.

[27] Y.S. Kang, S. Risbud, J.F. Rabolt, P. Stroeve, Synthesis and characterization of nanometer-size Fe_3O_4 and γ-Fe_2O_3 particles, Chem. Mater. 8 (1996) 2209–2211, https://doi.org/10.1021/cm960157j.

[28] A. Anantharaman, Y. Chun, T. Hua, J.W. Chew, R. Wang, Pre-deposited dynamic membrane filtration – a review, Water Res. 173 (2020) 115558, https://doi.org/10.1016/j.watres.2020.115558.

[29] F.C. Kramer, R. Shang, L.C. Rietveld, S.J.G. Heijman, Influence of pH, multivalent counter ions, and membrane fouling on phosphate retention during ceramic nanofiltration, Separ. Purif. Technol. 227 (2019) 115675, https://doi.org/10.1016/j.seppur.2019.115675.

[30] D. Haldar, P. Duarah, M.K. Purkait, MOFs for the treatment of arsenic, fluoride and iron contaminated drinking water: a review, Chemosphere 251 (2020) 126388, https://doi.org/10.1016/j.chemosphere.2020.126388.

[31] J.C. Mailen, O.K. Tallent, P.C. Arwood, Destruction of Oxalate by Reaction with Hydrogen Peroxide, INIS, United States, 1981, p. 30.

[32] H. Huang, T. Young, J.G. Jacangelo, Novel approach for the analysis of bench-scale, low pressure membrane fouling in water treatment, J. Membr. Sci. 334 (2009) 1–8, https://doi.org/10.1016/j.memsci.2009.01.049.

[33] B. Tang, G. Wang, L. Zhuo, J. Ge, L. Cui, Facile route to α-FeOOH and α-Fe_2O_3 nanorods and magnetic property of α-Fe_2O_3 nanorods, Inorg. Chem. 45 (2006) 5196–5200, https://doi.org/10.1021/ic060097b.

[34] D. Lu, W. Cheng, T. Zhang, X. Lu, Q. Liu, J. Jiang, J. Ma, Hydrophilic Fe_2O_3 dynamic membrane mitigating fouling of support ceramic membrane in ultrafiltration of oil/water emulsion, Separ. Purif. Technol. 165 (2016) 1–9, https://doi.org/10.1016/j.seppur.2016.03.034.

[35] L. Song, M. Elimelech, Theory of concentration polarization in crossflow filtration, J. Chem. Soc. Faraday. Trans. 91 (1995) 3389–3398, https://doi.org/10.1039/FT9959103389.

[36] G.S. Ajmani, D. Goodwin, K. Marsh, D.H. Fairbrother, K.J. Schwab, J.G. Jacangelo, H. Huang, Modification of low pressure membranes with carbon nanotube layers for fouling control, Water Res. 46 (2012) 5645–5654, https://doi.org/10.1016/j.watres.2012.07.059.

[37] Y. Zhao, Y. Tan, F.-S. Wong, A.G. Fane, N. Xu, Formation of dynamic membranes for oily water separation by crossflow filtration, Separ. Purif. Technol. 44 (2005) 212–220, https://doi.org/10.1016/j.seppur.2005.01.010.

[38] L. Wang, R. Miao, X. Wang, Y. Lv, X. Meng, Y. Yang, D. Huang, L. Feng, Z. Liu, K. Ju, Fouling behavior of typical organic foulants in polyvinylidene fluoride ultrafiltration membranes: characterization from microforces, Environ. Sci. Technol. 47 (2013) 3708–3714, https://doi.org/10.1021/es4004119.

[39] E. Zuriaga-Agustí, E. Alventosa-deLara, S. Barredo-Damas, M.I. Alcaina-Miranda, M.I. Iborra-Clar, J.A. Mendoza-Roca, Performance of ceramic ultrafiltration membranes and fouling behavior of a dye-polysaccharide binary system, Water Res. 54 (2014) 199–210, https://doi.org/10.1016/j.watres.2014.01.064.

[40] R.W. Field, D. Wu, J.A. Howell, B.B. Gupta, Critical flux concept for microfiltration fouling, J. Membr. Sci. 100 (1995) 259–272, https://doi.org/10.1016/0376-7388(94)00265-Z.

[41] I. Katsounaros, W.B. Schneider, J.C. Meier, U. Benedikt, P.U. Biedermann, A. A. Auer, K.J.J. Mayrhofer, Hydrogen peroxide electrochemistry on platinum: towards understanding the oxygen reduction reaction mechanism, Phys. Chem. Chem. Phys. 14 (2012) 7384–7391, https://doi.org/10.1039/C2CP40616K.

[42] S. Gligorovski, R. Strekowski, S. Barbati, D. Vione, Environmental implications of hydroxyl radicals (•OH), Chem. Rev. 115 (2015) 13051–13092, https://doi.org/10.1021/cr500310b.

[43] E. Brillas, I. Sirés, M.A. Oturan, Electro-Fenton process and related electrochemical technologies based on Fenton's reaction chemistry, Chem. Rev. 109 (2009) 6570–6631, https://doi.org/10.1021/cr900136g.

[44] L. Chen, J. Ma, X. Li, J. Zhang, J. Fang, Y. Guan, P. Xie, Strong enhancement on Fenton oxidation by addition of hydroxylamine to accelerate the ferric and ferrous iron cycles, Environ. Sci. Technol. 45 (2011) 3925–3930, https://doi.org/10.1021/es2002748.

[45] C.K. Duesterberg, S.E. Mylon, T.D. Waite, pH effects on iron-catalyzed oxidation using Fenton's reagent, Environ. Sci. Technol. 42 (2008) 8522–8527, https://doi.org/10.1021/es801720d.

[46] S.-S. Lin, M.D. Gurol, Catalytic decomposition of hydrogen peroxide on iron oxide: Kinetics, mechanism, and implications, Environ. Sci. Technol. 32 (1998) 1417–1423, https://doi.org/10.1021/es970648k.

[47] S.G. Huling, P.K. Jones, T.R. Lee, Iron optimization for Fenton-driven oxidation of MTBE-spent granular activated carbon, Environ. Sci. Technol. 41 (2007) 4090–4096, https://doi.org/10.1021/es062666k.

[48] W.S. Ang, A. Tiraferri, K.L. Chen, M. Elimelech, Fouling and cleaning of RO membranes fouled by mixtures of organic foulants simulating wastewater effluent, J. Membr. Sci. 376 (2011) 196–206, https://doi.org/10.1016/j.memsci.2011.04.020.

[49] N.S. Kaisheva, A.S. Kaishev, Potentiometric titration for determining the composition and stability of metal(II) alginates and pectinates in aqueous solutions, Russ. J. Phys. Chem. 89 (2015) 1216–1222, https://doi.org/10.1134/S0036024415070146.

[50] R.M. Smith, A.E. Martell, Critical stability constants, enthalpies and entropies for the formation of metal complexes of aminopolycarboxylic acids and carboxylic acids, Sci. Total Environ. 64 (1987) 125–147, https://doi.org/10.1016/0048-9697(87)90127-6.

[51] G. Mustafa, K. Wyns, A. Buekenhoudt, V. Meynen, New insights into the fouling mechanism of dissolved organic matter applying nanofiltration membranes with a variety of surface chemistries, Water Res. 93 (2016) 195–204, https://doi.org/10.1016/j.watres.2016.02.030.

[52] Y. Lester, D. Avisar, H. Mamane, Ozone degradation of cyclophosphamide – effect of alkalinity and key effluent organic matter constituents, Ozone Sci. Eng. 35 (2013) 125–133, https://doi.org/10.1080/01919512.2013.761107.

[53] X. Xue, K. Hanna, C. Despas, F. Wu, N. Deng, Effect of chelating agent on the oxidation rate of PCP in the magnetite/H_2O_2 system at neutral pH, J. Mol. Catal. Chem. 311 (2009) 29–35, https://doi.org/10.1016/j.molcata.2009.06.016.

[54] F.C. Kramer, R. Shang, L.C. Rietveld, S.J.G. Heijman, Fouling control in ceramic nanofiltration membranes during municipal sewage treatment, Separ. Purif. Technol. 237 (2020) 116373, https://doi.org/10.1016/j.seppur.2019.116373.

[55] Y. Pan, W. Wang, W. Wang, T. Wang, Prediction of particle deposition and layer growth in the preparation of a dynamic membrane with cross-flow microfiltration, RSC Adv. 5 (2015) 89015–89024, https://doi.org/10.1039/C5RA14572D.

[56] W. Kim, C.-Y. Suh, S.-W. Cho, K.-M. Roh, H. Kwon, K. Song, I.-J. Shon, A new method for the identification and quantification of magnetite–maghemite mixture using conventional X-ray diffraction technique, Talanta 94 (2012) 348–352, https://doi.org/10.1016/j.talanta.2012.03.001.

[57] S. Anisah, W. Puthai, M. Kanezashi, H. Nagasawa, T. Tsuru, Preparation, characterization, and evaluation of TiO_2-ZrO_2 nanofiltration membranes fired at different temperatures, J. Membr. Sci. 564 (2018) 691–699, https://doi.org/10.1016/j.memsci.2018.07.072.

[58] M.T. Alresheedi, O.D. Basu, B. Barbeau, Chemical cleaning of ceramic ultrafiltration membranes – ozone versus conventional cleaning chemicals, Chemosphere 226 (2019) 668–677, https://doi.org/10.1016/j.chemosphere.2019.03.188.

[59] D.M. Cwiertny, G.J. Hunter, J.M. Pettibone, M.M. Scherer, V.H. Grassian, Surface chemistry and dissolution of α-FeOOH nanorods and microrods: environmental implications of size-dependent interactions with oxalate, J. Phys. Chem. C 113 (2009) 2175–2186, https://doi.org/10.1021/jp807336t.

[60] T. Xu, R. Zhu, H. Shang, Y. Xia, X. Liu, L. Zhang, Photochemical behavior of ferrihydrite-oxalate system: interfacial reaction mechanism and charge transfer process, Water Res. 159 (2019) 10–19, https://doi.org/10.1016/j.watres.2019.04.055.

[61] L.S. Darken, The ionization constants of oxalic acid at 25° from conductance measurements, J. Am. Chem. Soc. 63 (1941) 1007–1011, https://doi.org/10.1021/ja01849a033.

[62] E.M. Rodríguez, G. Fernández, P.M. Álvarez, R. Hernández, F.J. Beltrán, Photocatalytic degradation of organics in water in the presence of iron oxides: effects of pH and light source, Appl. Catal. B Environ. 102 (2011) 572–583, https://doi.org/10.1016/j.apcatb.2010.12.041.

[63] C. Liu, W. Leng, P.J. Vikesland, Controlled evaluation of the impacts of surface coatings on silver nanoparticle dissolution rates, Environ. Sci. Technol. 52 (2018) 2726–2734, https://doi.org/10.1021/acs.est.7b05622.

[64] Y. Nakamura, M. Daidai, F. Kobayashi, Ozonolysis mechanism of lignin model compounds and microbial treatment of organic acids produced, Water Sci. Technol. 50 (2004) 167–172, https://doi.org/10.2166/wst.2004.0188.